

NASA Contractor Report 189549
ICASE Report No. 91-78

IN-64
48398
P. 29

ICASE

ENERGY MODELS FOR ONE-CARRIER TRANSPORT IN SEMICONDUCTOR DEVICES

(NASA-CR-189549) ENERGY MODELS FOR
ONE-CARRIER TRANSPORT IN SEMICONDUCTOR
DEVICES Final Report (ICASE) 29 p CSCL 12A

N92-12557

Unclas
G3/64 0048398

Joseph W. Jerome
Chi-Wang Shu

Contract No. NAS1-18605
October 1991

Institute for Computer Applications in Science and Engineering
NASA Langley Research Center
Hampton, Virginia 23665-5225

Operated by the Universities Space Research Association



National Aeronautics and
Space Administration

Langley Research Center
Hampton, Virginia 23665-5225

ERRATA

NASA Contractor Report 189046

ENERGY MODELS FOR ONE-CARRIER TRANSPORT
IN SEMICONDUCTOR DEVICES

Joseph W. Jerome and Chi-Wang Shu

October 1991

NASA Contractor Report 189046 has an incorrect report number. The correct report number is NASA Contractor Report 189549. Please mark your copies on the cover and Report Documentation Page to reflect this change.

Issued January 1992

ENERGY MODELS FOR ONE-CARRIER TRANSPORT IN SEMICONDUCTOR DEVICES

Joseph W. Jerome¹

Department of Mathematics
Northwestern University
Evanston, IL 60208

Chi-Wang Shu²

Division of Applied Mathematics
Brown University
Providence, RI 02912

ABSTRACT

Moment models of carrier transport, derived from the Boltzmann equation, have made possible the simulation of certain key effects through such realistic assumptions as energy dependent mobility functions. This type of global dependence permits the observation of velocity overshoot in the vicinity of device junctions, not discerned via classical drift-diffusion models, which are primarily local in nature. It has been found that a critical role is played in the hydrodynamic model by the heat conduction term. When ignored, the overshoot is inappropriately damped. When the standard choice of the Wiedemann-Franz law is made for the conductivity, spurious overshoot is observed. Agreement with Monte-Carlo simulation in this regime has required empirical modification of this law, as observed by IBM researchers, or nonstandard choices. In this paper, simulations of the hydrodynamic model in one and two dimensions, as well as simulations of a newly developed energy model, the RT model, will be presented. The RT model, intermediate between the hydrodynamic and drift-diffusion model, was developed at the University of Illinois to eliminate the parabolic energy band and Maxwellian distribution assumptions, and to reduce the spurious overshoot with physically consistent assumptions. The algorithms employed for both models are the essentially non-oscillatory shock capturing algorithms, developed at UCLA during the last decade. Some mathematical results will be presented, and contrasted with the highly developed state of the drift-diffusion model.

¹The first author is supported by the National Science Foundation under Grant DMS-8922398.

²This research was supported in part by the National Aeronautics and Space Administration under NASA Contract No. NAS1-18605 while the second author was in residence at the Institute for Computer Applications in Science and Engineering (ICASE), NASA Langley Research Center, Hampton, VA 23665. Additional support was also provided by Army Research Office under Grant DAAL03-91-G-0123 and by the National Aeronautics and Space Administration under Grant NAG1-1145.

1 Introduction

During the last decade, device modeling has attempted to incorporate general carrier heating, velocity overshoot, and various small device features into carrier simulation. The popular wisdom emerging from such concentrated study holds that global dependence of critical quantities, such as mobilities, on energy and/or temperature, is essential if such phenomena are to be modeled adequately. In this paper, we examine in detail the simulation of two such energy models, including the hydrodynamic model and the RT model. We describe the models, summarize some associated mathematical results, as well as the basic features of the numerical algorithm, and then present the results of extensive numerical simulations for two-dimensional MESFET devices, and for one-dimensional diodes. Both models represent one carrier flow. The hydrodynamic model contains hyperbolic modes related to the momentum equations, while the RT model does not possess such modes. In both cases, however, we employ a conservation law format, and numerical methods suitable for such systems. The ENO (essentially non-oscillatory) method employed makes use of adaptive stencils, and is particularly adept at shock capturing if the parameter regime crosses from supersonic to subsonic. Even if this does not occur, the convective terms are effectively discretized, via this procedure, in both models. The first use of such methods in device simulation was in [7], followed by the study [6], in which shocks were detected in micron devices at liquid Nitrogen temperatures, and at room temperature in shorter devices, by independent numerical techniques.

Our development of the RT model follows that of [5]. These researchers attempted to utilize a microscopic relaxation time approximation, which would allow for nonparabolic energy bands and non-Maxwellian distribution functions. The approach allows for parameter fitting of certain key quantities via Monte-Carlo simulation.

One of the principal conclusions of the paper is the essential dependence of the hydrodynamic model upon the heat conduction term. Standard choices lead to numerically detected spurious overshoot at the drain junction of an $n^+ - n - n^+$ diode, while other choices significantly damp this overshoot. Monte-Carlo simulations show that substantial underestimation occurs when the heat conduction term is neglected. We refer the reader to [10], and to the simulation results of this paper for amplification. The RT model was developed, partly in response to the continuing debate concerning heat conduction processes in the hydrodynamic model.

The status of mathematical results differs sharply between the hydrodynamic model, on the one hand, and the drift-diffusion model on the other. For the former, we have summarized two results, one by Gamba (cf. [8]) for an idealized model, in which the adi-

abatic relation is employed, and another by Gardner, Jerome, and Rose (cf. [9]) in which a Newton-Kantorovich theorem is developed for the $n^+ - n - n^+$ diode, yielding existence and convergence in a specialized subsonic regime. The drift-diffusion model, on the other hand, has been widely studied. Existence and approximation results have been carefully developed, although uniqueness is still not well understood for this model. Existence for the steady-state model is due in varying degrees of generality to many authors, including Mock ([17]), Seidman ([21]), and the first author ([13]). A convergence theory, based upon a calculus due to Krasnosel'skii, was presented in ([15]). Mathematical results have not yet been developed for the strongly nonlinear RT model.

2 Hydrodynamic and Drift-Diffusion Models

2.1 Mass, momentum and energy transport equations

The equations as presented here are discussed in references [3], [20], and [4]. They are derived as the first three moments of the Boltzmann equation, with the latter written for electrons moving in an electric field as

$$\frac{\partial f}{\partial t} + u \cdot \nabla_x f - \frac{e}{m} F \cdot \nabla_u f = C. \quad (1)$$

Here, $f = f(x, u, t)$ is the numerical distribution function of a carrier species, x is the position vector, u is the species' group velocity vector, $F = F(x, t)$ is the electric field, e is the electron charge modulus, m is the effective electron mass, and C is the time rate of change of f due to collisions. In the Boltzmann equation above, it has been assumed that the traditional Lorentz force field does not have a component induced by an external magnetic field. The moment equations, which will be derived subsequently, are expressed in terms of certain dependent variables, where n is the electron concentration, v is the average velocity, p is the momentum density, P is the symmetric pressure tensor, q is the the heat flux, e_I is the internal energy, and C_n , C_p , and C_W represent moments of C , taken with respect to the functions

$$\begin{aligned} h_0(u) &\equiv 1, \\ h_1(u) &= mu, \\ h_2(u) &= \frac{m}{2} |u|^2. \end{aligned}$$

The equations are given by:

$$\frac{\partial n}{\partial t} + \nabla \cdot (nv) = C_n, \quad (2)$$

$$\frac{\partial p}{\partial t} + v(\nabla \cdot p) + (p \cdot \nabla)v = -enF - \nabla \cdot P + C_p, \quad (3)$$

$$\begin{aligned} \frac{\partial}{\partial t} \left(\frac{mn}{2} |v|^2 + mne_I \right) + \nabla \cdot \left(v \left\{ \frac{mn}{2} |v|^2 + mne_I \right\} \right) = \\ - env \cdot F - \nabla \cdot (vP) - \nabla \cdot q + C_W. \end{aligned} \quad (4)$$

The first Maxwell equation for the electric potential must be adjoined; each species contributes a corresponding moment subsystem, with appropriately signed charge. We begin the derivation with the definitions and assumptions. The concentration is given by $n := \int f \, du$; the average velocity by $v := \frac{1}{n} \int u f \, du$; the momentum by $p := mnv$; the random velocity by $c := u - v$; the pressure tensor by $P_{ij} := m \int c_i c_j f \, du$; and the internal energy density by $e_I := \frac{1}{2n} \int |c|^2 f \, du$. This function represents energy/unit mass/unit concentration. The heat flux q is given by $q_i := \frac{m}{2} \int c_i |c|^2 f \, du$. Finally, for reference in subsequent subsections, the electron current density is given by $J := -env$, and the energy flux is given by $S := \int u \left\{ \frac{m}{2} |u|^2 \right\} f \, du$. The assumptions on f are now stated. The function f is assumed to decrease sufficiently rapidly at infinity:

$$\lim_{|u| \rightarrow \infty} h_i(u) f(u) = 0, \quad i = 0, 1, 2.$$

The derivation of (2), (3), (4) proceeds by multiplying the Boltzmann equation (1) by h_0, h_1 , and h_2 , respectively, and integrating over group velocity space. With the application of certain standard identities ([16]), the mass/momentum/energy system is obtained. In addition to these transport equations, we have Poisson's equation for the electric field, where $n_d :=$ doping and $\epsilon :=$ dielectric:

$$F = -\nabla \phi, \quad (5)$$

$$\nabla \cdot (\epsilon \nabla \phi) = -\sum e_i n_i - n_d. \quad (6)$$

Here, we have used the convention that there are different species, each of concentration n_i and charge e_i . The entire system consists of equations (2), (3), (4), repeated according to species, and (5), (6).

2.2 Moment closure and relaxation relations

The system derived in the preceding subsection has fifteen dependent variables in the case of one species, determined by ϕ, n, v, P, e_I , and q . By moment closure is meant the selection of compatible relations among these variables, so that the number of equations is equal in number to the remaining primitive variables selected. The relations to follow are characterized by the isotropic/parabolic energy band assumption. We begin by introducing a new tensor variable T , the carrier temperature, defined by

$$P_{ij} = nkT_{ij}$$

where k is Boltzmann's constant, and a scalar variable W , the total carrier energy. A program of reduction to a set of basic variables, n , v , W , and ϕ , or a set equivalent to these, can be implemented by the following assumptions:

- The pressure tensor is isotropic, with diagonal entries P_s and off-diagonal entries zero, for a suitable scalar function, P_s . P_s is related to e_I via $mne_I = \frac{3}{2}P_s$.
- It follows from the previous assumption that temperature may be represented by a scalar quantity T , and that the internal energy is represented in terms of T by

$$me_I = \frac{3}{2}kT.$$

- The total energy density (per unit concentration) w is given by combining internal energy and parabolic energy bands with m assumed constant:

$$w = me_I + \frac{1}{2}m |v|^2,$$

and the total energy (per unit volume) W is the product, $W = nw$.

- The heat flux is obtained by a differential expression involving the temperature:

$$q = -\kappa \nabla T.$$

Here, κ is the thermal conductivity governed by the Wiedemann-Franz law (cf. [2]), described by

$$\kappa = \left(\frac{5}{2} + r\right)n \frac{k^2 \mu_0}{e} T \left(\frac{T}{T_0}\right)^r. \quad (7)$$

The standard choice for r is $r = -1$, but this has some associated difficulties. This will be amplified later in the paper. Here we simply remark that the term raised to the exponent r in (7) is proportional to the mobility, which in turn is proportional to the momentum relaxation time.

In the case of N species, the closure relations determine $(d + 2)N + 1$ variables in d spatial dimensions. It is possible to rewrite the system (2, 3, 4) with the closure assumptions incorporated. We have the following.

$$\frac{\partial n}{\partial t} + \nabla \cdot (nv) = C_n, \quad (8)$$

$$\frac{\partial p}{\partial t} + v(\nabla \cdot p) + (p \cdot \nabla)v = -enF - \nabla \cdot (nkT) + C_p, \quad (9)$$

$$\begin{aligned} \frac{\partial W}{\partial t} + \nabla \cdot (vW) &= -env \cdot F - \nabla \cdot (vnkT) \\ &+ \nabla \cdot (\kappa \nabla T) + C_w. \end{aligned} \quad (10)$$

The final step deals with the replacement of the collision moments. Motivated by the approach of [18], [1], [20], and [11], we define the recombination rate R and the momentum and energy relaxation times, τ_p and τ_w , respectively, in terms of averaged collision moments as follows.

1. The particle recombination rate R is given by

$$R := -C_n := - \int C \, du.$$

2. The momentum relaxation time τ_p is given via

$$\frac{p}{\tau_p} := -m \int u C \, du := -C_p.$$

3. The energy relaxation time τ_w is given via

$$-\frac{W - W_0}{\tau_w} := \frac{m}{2} \int |u|^2 f \, du := C_W.$$

Here, W_0 denotes the rest energy, $\frac{3}{2}kT_0$, where T_0 is the lattice temperature.

The forms for the relaxation times used in [1] and retained by subsequent authors are:

$$\tau_p = c_p \left(\frac{T}{T_0}\right)^r, \quad (11)$$

$$\tau_w = c_w \frac{T}{T + T_0} + \frac{1}{2}\tau_p. \quad (12)$$

Here, c_p and c_w are physical constants, and the standard choice for r , just as in (2.7), is -1 .

2.3 Drift-diffusion model

The drift-diffusion model may be obtained by taking zeroth order moments of the BTE and adjoining the Poisson equation. Thus, one obtains the system for N carriers with concentrations n_i and charge e_i , $i = 1, \dots, N$:

$$\frac{\partial n_i}{\partial t} + \nabla \cdot J_i = -R_i, \quad (13)$$

$$F = -\nabla \phi, \quad (14)$$

$$\nabla \cdot (\epsilon \nabla \phi) = -\sum e_i n_i - n_d. \quad (15)$$

There still remains the issue of determining the constitutive current relations. Classical drift-diffusion theory gives, for $N = 2$, $n_1 = n$, and $n_2 = p$,

$$J_n = -e\mu_n n \nabla \phi + eD_n \nabla n, \quad (16)$$

$$J_p = -e\mu_p p \nabla \phi - eD_p \nabla p. \quad (17)$$

The introduction of exponential relations for n and p is also common, as is the use of the Einstein relations linking the mobilities, μ_n, μ_p , and the diffusion coefficients D_n, D_p . These relations are specified by

$$D_n = (kT/e)\mu_n, \quad (18)$$

$$D_p = (kT/e)\mu_p. \quad (19)$$

It is also possible to derive the constitutive relations (16), (17), from the first order moment relations under the assumption that the momentum relaxation times tend to zero. The details are given in [20]. In fact, the constitutive relations include a heat flux term as well, which is suppressed at constant temperature. If it is not suppressed, one has an energy drift-diffusion model. In this derivation, one uses the definition of mobility in terms of relaxation time.

3 RT Models

In this section, we shall employ a microscopic assumption upon the momentum relaxation time, viz. , we shall assume that the collision term C in (1) is of the form,

$$C = -\frac{f_1}{\tau_p}, \quad (20)$$

where f_1 is the odd part of f . Note that this contrasts with the macroscopic assumption on τ_p , employed in the hydrodynamic model as described in Section 2. There, the representation defining τ_p was a post averaged expression. Here, the expression is employed in the averaging. In this case, we may obtain an expression for the energy flux S :

$$S = -[n\mu^E F + \nabla(nD^E)], \quad (21)$$

where μ^E and D^E are tensor expressions for mobility and diffusion, defined in terms of moments, and E represents average energy per unit concentration. The details are furnished in [5]. It is also shown there that the current density has the usual drift-diffusion form, with tensor expressions for mobility and diffusion. The RT model makes the following microscopic assumptions, with distinction between \mathcal{E} and its average, E .

1. The even part of f is isotropic, and a function of \mathcal{E} alone, and the relaxation time is an inverse power function of \mathcal{E} :

$$\begin{aligned} f_0 &= f_0(\mathcal{E}), \\ \tau_p &= \tau_p(\mathcal{E}) = C\mathcal{E}^{-r}. \end{aligned}$$

2. The microscopic kinetic energy is a quadratic function of \mathcal{E} , and the mass is not assumed constant:

$$G(\mathcal{E}) := \frac{m^*}{2} |u|^2 = \mathcal{E} + \alpha\mathcal{E}^2, \quad (22)$$

where α is an appropriate fitting parameter.

3. The temperature is a modified variable in terms of which the following constitutive relation holds for E :

$$E = \frac{3}{2}kT(1 + \frac{5}{2}\alpha kT). \quad (23)$$

Equation (23) allows for nonparabolic energy bands as well as non-Maxwellian distributions. Altogether, the model may be written in terms of the Poisson equation, (6), in conjunction with the system,

$$\nabla \cdot J = 0, \quad (24)$$

$$\nabla \cdot S = J \cdot F - n \left\langle \frac{\partial E}{\partial t} \right\rangle_{coll}. \quad (25)$$

Here, J and S have been described previously, the latter in (21). In the expressions for J and S , the assumptions made for the model lead to scalar representations for the mobility and diffusion coefficients. For example, the choice made in [5] leads to

$$\mu = \mu_0 T_0 / T, \quad (26)$$

$$\mu^E = \frac{3}{2} \left(1 - \frac{\alpha}{2} kT\right) \mu kT. \quad (27)$$

The diffusion coefficients are defined by Einstein's relations. The collision term in (25) is a specified quadratic function of T . One significant advantage of the microscopic relaxation time (RT) assumption is that certain key parameters may be fitted via Monte-Carlo preprocessing, ensuring reliability of their values.

4 Mathematical Results for the Hydrodynamic Model

In this section, we shall describe some recent mathematical results, obtained in one spatial dimension. In the first subsection, we shall present existence and boundary layer results for a simplified version of the steady state hydrodynamic model. This will be followed by a convergence analysis for Newton's method in the subsonic case.

4.1 Existence and boundary layer theory

We first write down the one dimensional evolution system in the case of a single carrier, in the absence of recombination.

$$\frac{\partial n}{\partial t} + \frac{\partial(nv)}{\partial x} = 0, \quad (28)$$

$$\frac{\partial p}{\partial t} + \frac{\partial(pv + knT)}{\partial x} = -enF - \frac{p}{\tau_p}, \quad (29)$$

$$\frac{\partial W}{\partial t} + \frac{\partial(vW + vknT)}{\partial x} = -envF + \frac{\partial(\kappa(\partial T)/(\partial x))}{\partial x} - \frac{W - W_0}{\tau_w}, \quad (30)$$

$$\epsilon \frac{\partial F}{\partial x} = -en - n_d. \quad (31)$$

The corresponding steady state system is obtained by setting the time derivatives equal to zero.

If we rewrite the second steady state equation by use of the pressure, P , we obtain the equation,

$$\frac{\partial(pv + P)}{\partial x} = -enF - \frac{p}{\tau_p}. \quad (32)$$

The approach of [8] is to eliminate the energy equation (30) from the system, and replace its role by a relation in the spirit of gas dynamics, i. e. by the constitutive relation,

$$P(n) = Kn^\gamma, \quad \gamma > 1. \quad (33)$$

When units are selected in which $e = 1$, $\epsilon = 1$, $m = 1$, and $K = 1$, we obtain the system, in which n and ϕ are the only dependent variables,

$$j := nv \equiv \text{constant}, \quad (34)$$

$$(F(n))_x := \left(\frac{j}{n} + n^\gamma\right)_x = -n\phi_x - \frac{j}{\tau_p} := -S(\phi_x, n), \quad (35)$$

$$\phi_{xx} = n - n_d. \quad (36)$$

One can nominally specify boundary conditions on n and ϕ at the endpoints of the device, taken here as the interval, $[0, 1]$. If the doping is such that the built-in potential is the same at both ends of the device, then we may take,

$$\phi(0) = 0, \quad \phi(1) = \phi_1, \quad (37)$$

for ϕ and

$$n(0) = n_0, \quad n(1) = n_1, \quad (38)$$

for n , where ϕ_1 must satisfy the following consistency relation with respect to j , n_0 , and n_1 :

$$\phi_1 = f(n_1, j) - f(n_0, j) + j \int_0^1 \frac{dx}{\tau(n, j)n(x)}. \quad (39)$$

Here,

$$f(n, j) = \frac{j^2}{2n^2} + \gamma n^{\gamma-2}. \quad (40)$$

It is shown in [8] that a weak solution exists for the system (34), (35), (36), satisfying the boundary conditions exactly, or, in lieu of this, satisfying precise limiting relationships. The result for ϕ is classical, because the equation is elliptic. The result for n is provisional, and is detailed now. If $j > 0$, there is a weak solution n such that the relation,

$$n = G + \alpha, \quad (41)$$

holds, where G is Hölder ($\frac{1}{2}$) continuous, and α is monotone increasing. Although n need not be of bounded variation, it is an entropy solution, in the sense that the function of x ,

$$H(n(x)) = (F(n(x)) - F(n_{min}))\text{signum}(n(x) - n_{min}) + Cx, \quad (42)$$

is monotone increasing. Here, n_{min} is a minimum (location) for F , and $C = \sup S$ over relevant arguments. The following precise statement is available for subsonic boundary conditions. If $n_0, n_1 > n_{min}$, then the following holds.

- Either

$$n(1) = n_1,$$

- or

$$\lim_{x \rightarrow 1^-} n(x)$$

exists, and is a supersonic value, i. e. , is less than n_{min} , and even less than the conjugate value of n_1 .

- Similarly, either

$$n(0) = n_0,$$

- or

$$\lim_{x \rightarrow 0^+} n(x)$$

exists and is not less than n_{min} .

In the second instance of both cases above, boundary layers occur, the one on the right involving transition through the supersonic regime.

4.2 Newton convergence theory

In this subsection, we order the basic variables as v , n , T , and ϕ , because of symmetry considerations. Dirichlet boundary conditions are imposed, on n , T , ϕ , with $n(x_{min}) = n(x_{max})$. In one dimension, the steady state equations are obtained from (28), (29), (30), and (31) by setting the time derivatives equal to zero. Dirichlet boundary conditions are imposed

in this subsection on n , T , and ϕ , with $n(x_{min}) = n(x_{max})$. Since, by the conservation of mass equation, $nv = j$, it follows that the boundary conditions for v are periodic. The map defined by bringing all terms to the left hand side of the steady state system is called Φ . The linearized equations thus assume the form, where the boundary conditions are homogeneous Dirichlet conditions for δn , δT , and $\delta\phi$, and the boundary conditions on δv are prescribed to be periodic,

$$\begin{bmatrix} 0 \\ 0 \\ -\frac{1}{n} \frac{d}{dx} \left(\kappa \frac{d\delta T}{dx} \right) \\ -\epsilon \frac{d^2 \delta \phi}{dx^2} \end{bmatrix} + \begin{bmatrix} A & B \\ C & D \end{bmatrix} \frac{d}{dx} \begin{bmatrix} \delta v \\ \delta n \\ \delta T \\ \delta \phi \end{bmatrix} + \begin{bmatrix} E & F \\ G & H \end{bmatrix} \begin{bmatrix} \delta v \\ \delta n \\ \delta T \\ \delta \phi \end{bmatrix} = f. \quad (43)$$

The (spatially) dependent eigenvalues of the *symmetric* matrix A are calculated to be

$$\lambda = \frac{1}{2} \left(n + \frac{T}{mn} \right) \pm \frac{1}{2} \sqrt{\left(n + \frac{T}{mn} \right)^2 - 4 \left(\frac{T}{m} - v^2 \right)}. \quad (44)$$

Here,

$$A = \begin{bmatrix} n & v \\ v & \frac{T}{mn} \end{bmatrix}, \quad (45)$$

and the smaller eigenvalue is positive if n and T are strictly positive, and if

$$v^2 < \frac{T}{m} = c^2. \quad (46)$$

This type of point in function space is termed a subsonic point. This case was first considered in [9], where damped Newton/standard finite difference methods were presented. When Newton's method is employed in this way, it is essential to determine conditions under which the linear increments are appropriately bounded. This is equivalent to uniform bounds for the operator derivative inverse maps, and represents one of the three properties for an (exact) operator Newton method to yield existence of a root and R -quadratic convergence. The other two are sufficient regularity, and a sufficiently small starting residual, as measured in the range space norm. Explicit representations of B , C , D and of F , G , H are given in [14]. Moreover, if the system map Φ , subject to appropriate Dirichlet boundary conditions on n , T , and ϕ , and periodic boundary conditions on v , accordingly has the domain $D_\Phi \subset X = \prod_1^2 W^{1,\infty} \times \prod_1^2 W^{2,\infty}$, and range in $Y = \prod_1^4 L^\infty$, then (46) will hold for every element in a closed ball $B_{r_0} \subset X$, centered at a subsonic element $u_0 \in X$, such that n and T are strictly positive, if r_0 is sufficiently small. It is appropriate to assume at the outset, then, that $D_\Phi \subset B_{r_0}$, so that every function point in D_Φ satisfies (46); we may also assume that n and T are uniformly bounded away from zero in this set.

The Lipschitz property of the map Φ' , where here we view the system (43) as the representation for $\Phi'(v, n, T, \phi)(z, \omega) = f$, with

$$z = (\delta v, \delta n), \quad \omega = (\delta T, \delta \phi), \quad f = (f_1, f_2), \quad (47)$$

is evident from the representation for Φ' .

The uniform inverse bounding proceeds as follows. As shown in [9], with the function spaces selected in this paper, the H^1 product norm of z can be estimated in terms of the L^2 norms of ω , ω' , and f_1 , under the conjunction of the hypothesis (46) and the $L^2 \times L^2$ coerciveness assumption,

$$\Lambda = E + E^* - \frac{dA}{dx} \text{ is uniformly positive definite.} \quad (48)$$

Here, E^* is the matrix transpose of E and the latter is defined by

$$E = \begin{bmatrix} \frac{dn}{dx} & \frac{dv}{dx} \\ \frac{dv}{dx} + \frac{1}{\tau_p} & \left(\frac{-1}{mn^2}\right) T \frac{dn}{dx} \end{bmatrix}. \quad (49)$$

A final calculation, making use of the inner product of $[0, \omega]$ with (43), and the hypothesis,

$$h_{11} \text{ is positive, and sufficiently large,} \quad (50)$$

where h_{11} is the nonzero entry of H , given by

$$h_{11} = \frac{dv}{dx} + \frac{\frac{dW}{dT} \tau_w - (W - W_0) \tau'_w}{\tau_w^2}, \quad (51)$$

with $\tau'_w = \frac{d\tau_w}{dT}$, shows that the H^1 product norm of $[z, \omega]$ is estimated in terms of the L^2 norm of f . This series of calculations controls the L^∞ norm of $[z, \omega]$; the L^∞ norm of $[z', \omega'']$ is now estimated by direct use of the system (43), making use of the fact that $[v, n, T, \phi] \in B_{r_0}$. We have now outlined the proof of the following.

Theorem 4.1 *Let the function spaces X and Y be selected as above, let the steady state system map Φ be given with Dirichlet boundary conditions on n, T, ϕ , and periodic boundary conditions on v , such that $D_\Phi \subset B_{r_0}$, where every point in B_{r_0} is a subsonic point, with uniform positivity bounds. If (48) and (51) hold, and x_0 is such that $\Phi(x_0)$ is sufficiently small, then an R -quadratically convergent Newton sequence $\{x_n\}$ may be defined in the standard way, with limit x , satisfying $\Phi(x) = 0$.*

5 Discrete Schemes Based on Adaptive Stencils: ENO

In this section, we shall briefly describe the ENO schemes as developed in [24] and [25]. Consider a system of hyperbolic conservation laws of the form

$$u_t + \sum_1^d f_i(u)_{x_i} = g(u, x, t), \quad (52)$$

where

$$u = (u_1, \dots, u_m)^T, \quad x = (x_1, \dots, x_m),$$

and the hyperbolicity condition,

$$\sum_1^d \xi_i \frac{\partial f_i}{\partial u} \text{ is diagonalizable, with real eigenvalues,}$$

holds for any real $\xi = (\xi_1, \dots, \xi_d)$. An initial condition is adjoined to (52).

For systems of conservation laws, local field by field decomposition is used, to resolve waves in different characteristic directions. Analytical expressions are employed for the eigenvalues and eigenvectors of an averaged Jacobian matrix. Typically, the Roe average [19] is employed. One feature of the ENO schemes in [24] and [25], which is distinct from the original ENO schemes of Harten et al [12], is that multidimensional regions are treated dimension by dimension: when computing $f_i(u)_{x_i}$ in any particular direction, variables in all other directions are kept constant, and the Jacobians are treated in this direction. This, in essence, reduces the determination of the scheme to the case of a single conservation law in one spatial dimension. Thus, to describe the schemes, consider the scalar one dimensional problem, and a conservative approximation of the spatial operator given by

$$L(u)_j = -\frac{1}{\Delta x} (\hat{f}_{j+\frac{1}{2}} - \hat{f}_{j-\frac{1}{2}}). \quad (53)$$

Here, the numerical flux \hat{f} is assumed consistent:

$$\hat{f}_{j+\frac{1}{2}} = \hat{f}(u_{j-l}, \dots, u_{j+k}); \quad \hat{f}(u, \dots, u) = f(u). \quad (54)$$

The conservative scheme (53), which characterizes the \hat{f} divided difference as an approximation to $f(u)_x$, suggests that \hat{f} can be identified with an appropriate function h satisfying

$$f(u(x)) = \int_{x-\frac{\Delta x}{2}}^{x+\frac{\Delta x}{2}} h(\xi) d\xi. \quad (55)$$

If H is any primitive of h , then h can be computed from H' . H itself can be constructed by Newton's divided difference method, beginning with differences of order one, since the

constant term is arbitrary. The necessary divided differences of H , of a given order, are expressed as constant multiples of those of f of order one lower. After the polynomial Q of degree $r + 1$ has been constructed, set

$$\hat{f}_{j+\frac{1}{2}} = \frac{d}{dx}Q(x)|_{x=x_{j+\frac{1}{2}}}, \quad (56)$$

to obtain an r th order method. The construction is based on an adaptive stencil in the following sense:

- One begins with an appropriate starting point to the left or right of the current “cell” by means of upwinding as determined by the sign of the derivative of a selected flux.
- As the order of the divided differences is increased, the divided differences themselves determine the stencil: the “smaller” divided difference is chosen from two possible choices at each stage, ensuring a smoothest fit.
- Lax-Friedrichs building blocks or Roe building blocks can both be used. For the latter, in cells with sonic points, a local Lax-Friedrichs building block is used to avoid expansion shocks.

Steady states are reached by explicit time stepping of arbitrary order; nonstandard high order Runge-Kutta methods exist [24] which preserve nonlinear stability of the first order Euler forward version under suitable CFL time step restrictions. The computer program is fully vectorized for computations on Cray supercomputers. For details of the efficient implementation, see [23].

6 Conservation Law Format for Hydrodynamic and RT Models

In this section, we shall specify the conservation law format for the two dimensional hydrodynamic model, and for the one dimensional RT model.

6.1 Hydrodynamic model conservation format

Define the vector of dependent variables as

$$u = (n, \sigma, \tau, W), \quad (57)$$

where $p = (\sigma, \tau)$. The system (8), (9), (10) can be written in the concise form, in two dimensions, as

$$u_t + f_1(u)_x + f_2(u)_y = c(u) + G(u, \phi) + (0, 0, 0, \nabla \cdot (\kappa \nabla T)). \quad (58)$$

The following identifications have been made in (58).

$$f_1(u) = \left(\frac{\sigma}{m}, \frac{2}{3} \left(\frac{\sigma^2}{mn} + W - \frac{\tau^2}{2mn} \right), \frac{\sigma\tau}{mn}, \frac{5\sigma W}{3mn} - \sigma \frac{\sigma^2 + \tau^2}{3m^2n^2} \right), \quad (59)$$

$$f_2(u) = \left(\frac{\tau}{m}, \frac{\sigma\tau}{mn}, \frac{2}{3} \left(\frac{\tau^2}{mn} + W - \frac{\sigma^2}{2mn} \right), \frac{5\tau W}{3mn} - \tau \frac{\sigma^2 + \tau^2}{3m^2n^2} \right), \quad (60)$$

$$c(u) = \left(0, -\frac{\sigma}{\tau_p}, -\frac{\tau}{\tau_p}, -\frac{W - W_0}{\tau_w} \right), \quad (61)$$

$$G(u) = \left(0, -enF_1, -enF_2, -enF \cdot v \right). \quad (62)$$

The eigenvalues and eigenvectors of f'_1 and f'_2 are known (cf. [23]), and are readily incorporated into the field by field decomposition required for the implementation of ENO.

6.2 RT conservation format

We shall present the conservation law form of the RT model. We begin with the vector form,

$$u_t + f(u)_x = g(u)_{xx} + h(u). \quad (63)$$

In equation (63),

$$u = \left(en, \frac{nE}{m} \right), \quad (64)$$

$$f(u) = \phi' n (e\mu(E), \mu^E(E) + D(E)), \quad (65)$$

$$g(u) = (nD(E), nD^E(E)), \quad (66)$$

$$h(u) = \left(0, en\mu(E)(\phi')^2 + \frac{e}{\epsilon}(n - n_d)nD(E) - n \left\langle \frac{\partial E}{\partial t} \middle|_{coll} \right\rangle \right). \quad (67)$$

It can be shown that the left hand side defines a hyperbolic system, since the eigenvalues of $f'(u)$ are real, for all positive n and T .

7 Numerical Simulation Results

We now present numerical simulation results for one carrier, two dimensional MESFET devices and one dimensional diodes. The third order ENO shock-capturing algorithm with Lax-Friedrichs building blocks, as described briefly in Section 5 and in more detail in [25], is applied to the hyperbolic part (the left hand side) of Equations (6.2) and (6.7). A nonlinearly stable third order Runge-Kutta time discretization [24] is used for the time evolution towards steady states. The forcing terms on the right hand side of (6.2) and (6.7) are treated in a time consistent way in the Runge-Kutta time stepping. The double derivative terms on the

right hand side of (6.2) and (6.7) are approximated by standard central differences owing to their dissipative nature. The Poisson equation (2.6) is solved by direct Gauss elimination for one spatial dimension and by Successive Over-Relaxation (SOR) or the Conjugate Gradient (CG) method for two spatial dimensions. Initial conditions are chosen as $n = n_d$ for the concentration, $T = T_0$ for the temperature, and $u = v = 0$ (two spatial dimensions) or $u = 0$ (one spatial dimension) for the velocities. A continuation method is used to reach the steady state: the voltage bias is taken initially as zero and is gradually increased to the required value, with the steady state solution of a lower biased case used as the initial condition for a higher one.

7.1 Two dimensional MESFET

We simulate, using the Hydrodynamic model (6.2)-(2.6), a two dimensional MESFET of the size $0.6 \times 0.2 \mu m^2$. The source and the drain each occupies $0.1 \mu m$ at the upper left and the upper right, respectively, with the gate occupying $0.2 \mu m$ at the upper middle (Figure 1, left). The doping is defined by $n_d = 3 \times 10^{17} cm^{-3}$ in $[0, 0.1] \times [0.15, 0.2]$ and in $[0.5, 0.6] \times [0.15, 0.2]$, and $n_d = 1 \times 10^{17} cm^{-3}$ elsewhere, with abrupt junctions (Figure 1, right). A uniform grid of 96×32 points is used. Notice that even if we may not have shocks in the solution, the initial condition $n = n_d$ is discontinuous, and the final steady state solution has a sharp transition around the junction. With the relatively coarse grid we use, the non-oscillatory shock capturing feature of the ENO algorithm is essential for the stability of the numerical procedure.

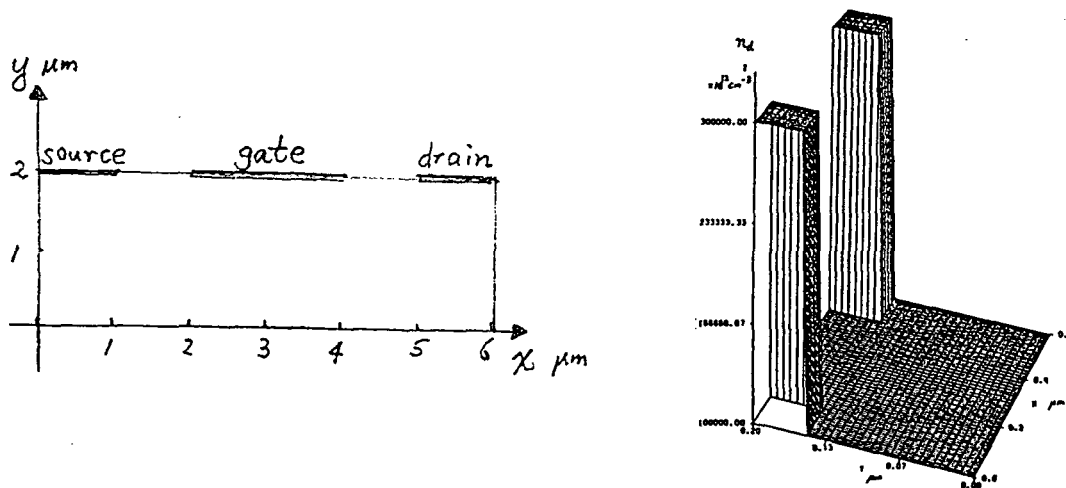


Figure 1: Two dimensional MESFET. Left: the geometry; Right: the doping n_d

We apply, at the source and drain, a voltage bias $v_{bias} = 2V$. The gate is a Schottky

contact, with a negative voltage bias $v_{gate} = -0.8V$ and a very low concentration value $n = 3.9 \times 10^5 cm^{-3}$ obtained from Equation (5.1-19) of [22]. The lattice temperature is taken as $T_0 = 300^\circ K$. The numerical boundary conditions are summarized as follows (where $\Phi_0 = \frac{k_b T}{e} \ln \left(\frac{n_d}{n_i} \right)$ with $k_b = 0.138 \times 10^{-4}$, $e = 0.1602$, and $n_i = 1.4 \times 10^{10} cm^{-3}$ in our units):

- At the source ($0 \leq x \leq 0.1, y = 0.2$): $\Phi = \Phi_0$ for the potential; $n = 3 \times 10^{17} cm^{-3}$ for the concentration; $T = 300^\circ K$ for the temperature; $u = 0 \mu m/ps$ for the horizontal velocity; and Neumann boundary condition for the vertical velocity v (i.e. $\frac{\partial v}{\partial \vec{n}} = 0$ where \vec{n} is the normal direction of the boundary).
- At the drain ($0.5 \leq x \leq 0.6, y = 0.2$): $\Phi = \Phi_0 + v_{bias} = \Phi_0 + 2$ for the potential; $n = 3 \times 10^{17} cm^{-3}$ for the concentration; $T = 300^\circ K$ for the temperature; $u = 0 \mu m/ps$ for the horizontal velocity; and Neumann boundary condition for the vertical velocity v .
- At the gate ($0.2 \leq x \leq 0.4, y = 0.2$): $\Phi = \Phi_0 + v_{gate} = \Phi_0 - 0.8$ for the potential; $n = 3.9 \times 10^5 cm^{-3}$ for the concentration; $T = 300^\circ K$ for the temperature; $u = 0 \mu m/ps$ for the horizontal velocity; and Neumann boundary condition for the vertical velocity v .
- At all other parts of the boundary ($0.1 \leq x \leq 0.2, y = 0.2$; $0.4 \leq x \leq 0.5, y = 0.2$; $x = 0, 0 \leq y \leq 0.2$; $x = 0.6, 0 \leq y \leq 0.2$; and $0 \leq x \leq 0.6, y = 0$), all variables are equipped with Neumann boundary conditions.

The boundary conditions chosen are based upon physical and numerical considerations. They may not be adequate mathematically, as is evident from some serious boundary layers observable in Figures 2 through 6. ENO methods, owing to their upwind nature, are robust to different boundary conditions (including over-specified boundary conditions) and do not exhibit numerical difficulties in the presence of such boundary layers, even with the extremely low concentration prescribed at the gate (around 10^{-12} relative to the high doping). We point out, however, that boundary conditions affect the global solution significantly. We have also simulated the same problem with different boundary conditions, for example with Dirichlet boundary conditions everywhere for the temperature, or with Neumann boundary conditions for all variables except for the potential at the contacts. The numerical results (not shown in this paper) are noticeably different. This indicates the importance of studying adequate boundary conditions, from both a physical and a mathematical point of view.

In Figures 2 through 6, we show pictures of the concentration n , temperature T , horizontal velocity u , vertical velocity v , and the potential Φ . Surfaces of the solution are shown at

the left, and cuts at $y = 0.175$, which cut through the middle of the high doping "blobs" horizontally, are shown at the right.

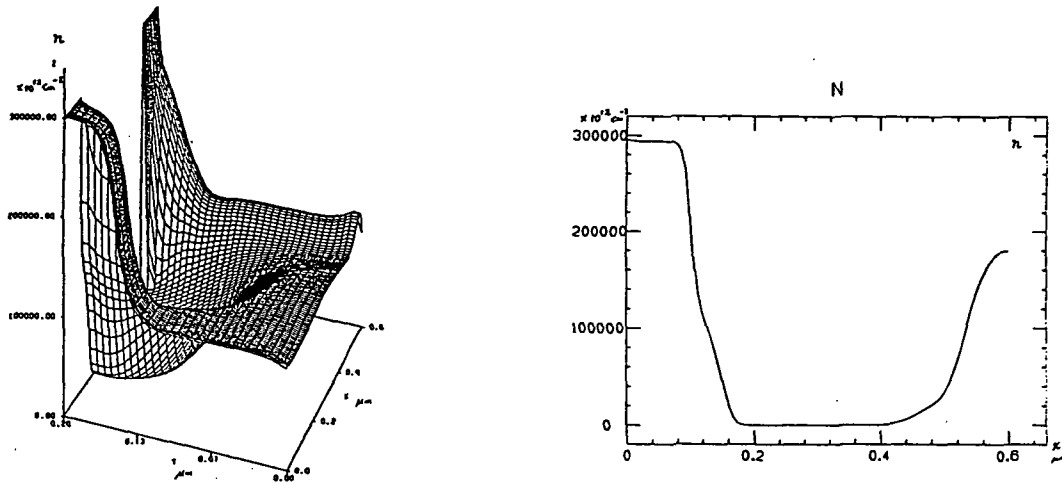


Figure 2: Two dimensional MESFET, concentration n . Left: surface of the solution; Right: cut at $y = 0.175$

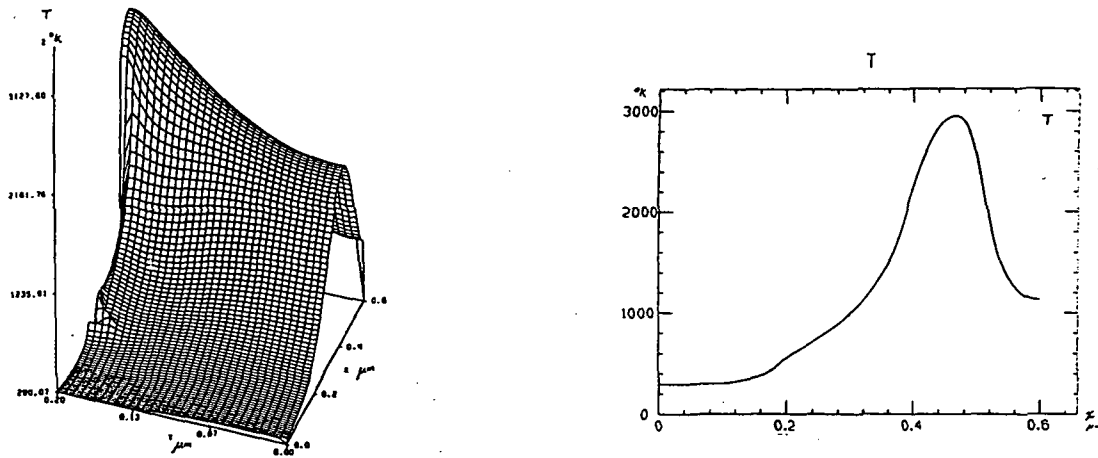


Figure 3: Two dimensional MESFET, temperature T . Left: surface of the solution; Right: cut at $y = 0.175$

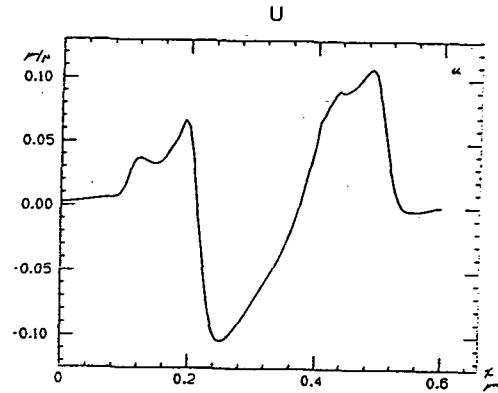
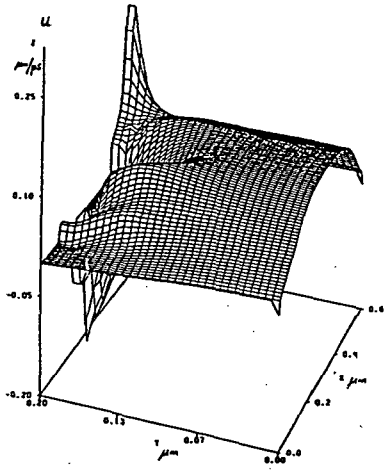


Figure 4: Two dimensional MESFET, horizontal velocity u . Left: surface of the solution; Right: cut at $y = 0.175$

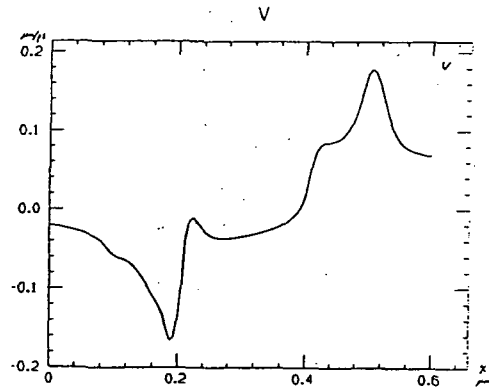
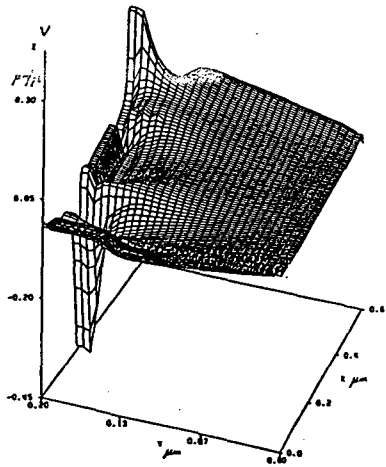


Figure 5: Two dimensional MESFET, vertical velocity v . Left: surface of the solution; Right: cut at $y = 0.175$

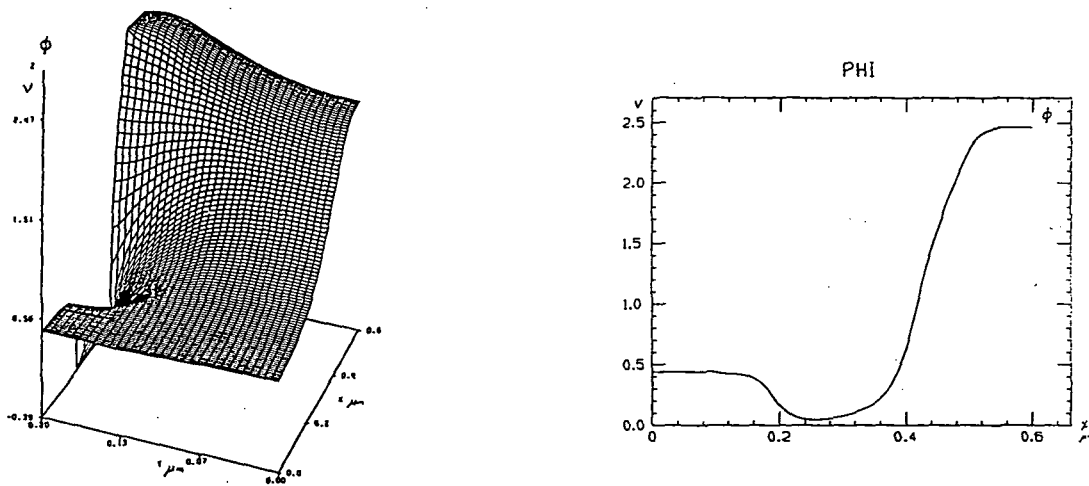


Figure 6: Two dimensional MESFET, potential Φ . Left: surface of the solution; Right: cut at $y = 0.175$

Notice that there is a boundary layer for the concentration n at the drain but not at the source. Also notice the rapid drop of n at the depletion region near the gate. The temperature achieves its maximum around the left corner of the drain. The leakage current at the gate appears negligible from the normal velocity component, while the horizontal component shows evidence of strong carrier movement toward the source beneath the left gate area, and strong movement toward the drain immediately to the left of the drain junction.

We have also simulated the same MESFET with a higher doping ratio: $3 \times 10^{17} \text{cm}^{-3}$ in the high doping region versus $1 \times 10^{15} \text{cm}^{-3}$ in the low doping region. We observe similar results (pictures not shown here).

7.2 HD model for a one dimensional diode — spurious velocity overshoot

A notorious phenomenon of HD models is that spurious velocity overshoot occurs at the drain junction of an $n^+ - n - n^+$ diode. It is intrinsic to the model and is not a numerical artifact, as is verified by our grid refinement study and by using different numerical algorithms. This phenomenon is closely related to the physical assumption governing the heat conduction term. Gnudi, Odeh and Rudan [10] observed that the spurious overshoot can be greatly reduced by an empirical modification of the Wiedemann-Franz law for the thermal conductivity.

In this subsection we perform an extensive numerical study of the dependency of the

spurious velocity overshoot upon the heat conduction term. The $n^+ - n - n^+$ diode we simulate has a length $0.6\mu\text{m}$, with a doping defined by $n_d = 3 \times 10^{17} \text{cm}^{-3}$ in $[0, 0.1]$ and in $[0.5, 0.6]$, and $n_d = 1 \times 10^{15} \text{cm}^{-3}$ in $[0.15, 0.45]$, with smooth junctions (Figure 7). The lattice temperature is taken as $T_0 = 296.21^\circ \text{K}$. We apply a voltage $v_{bias} = 1.5\text{V}$, as is the case in [10].

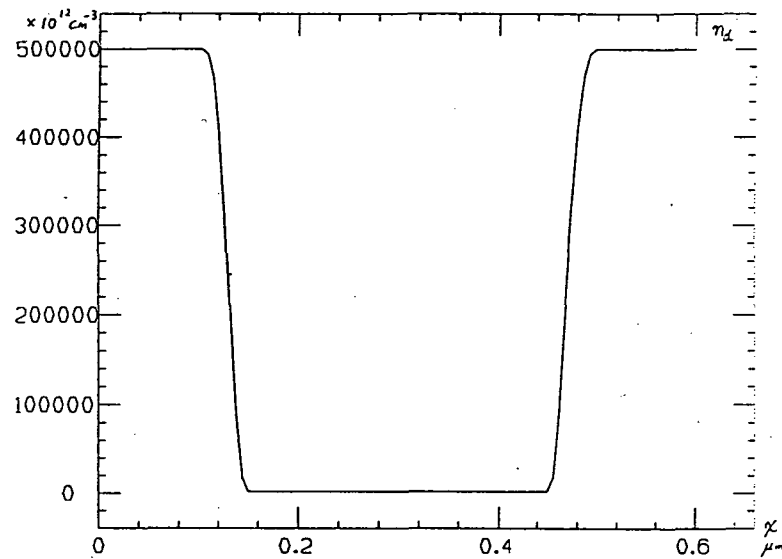


Figure 7: The doping n_d for the one dimensional $n^+ - n - n^+$ diode

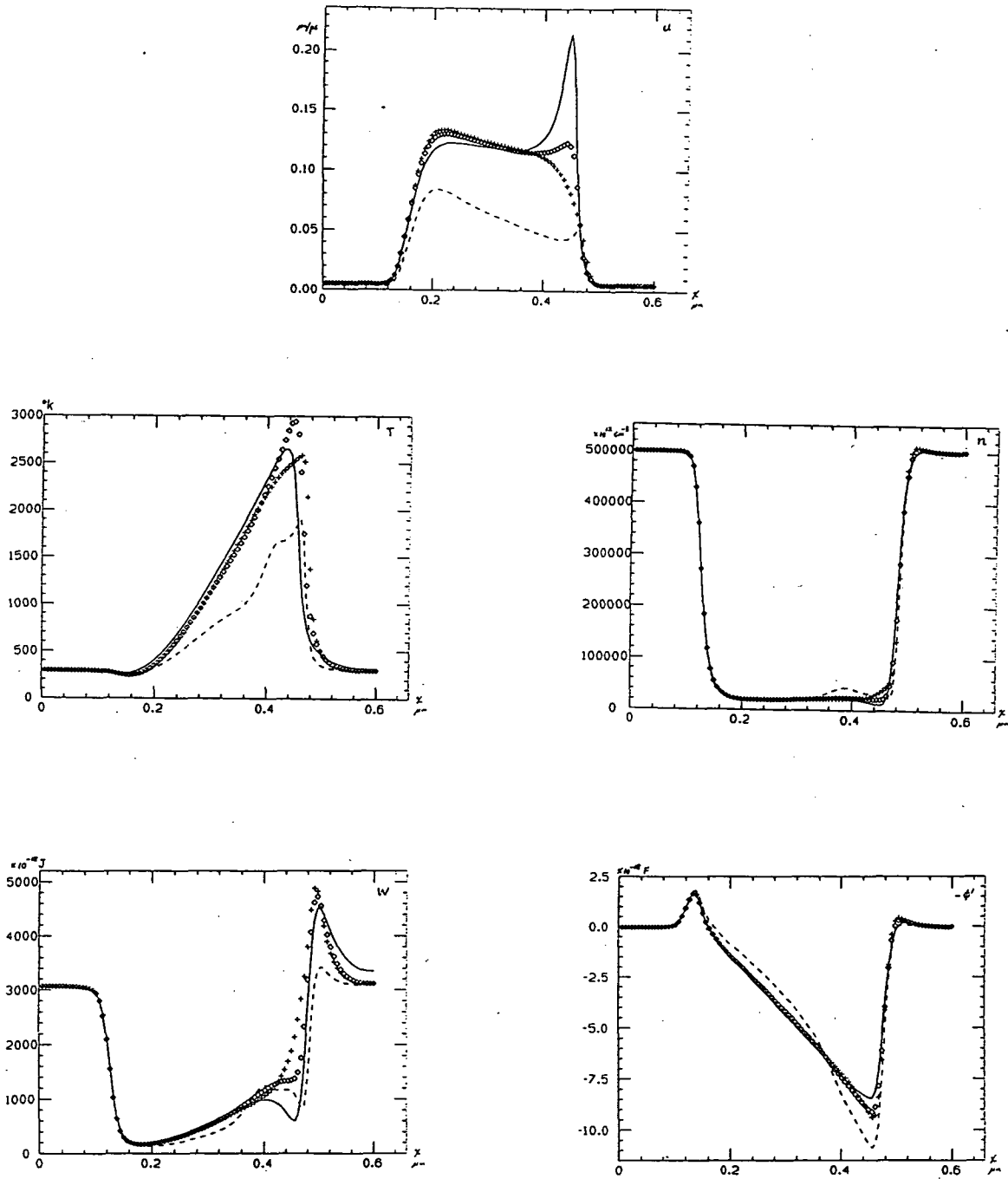


Figure 8: HD for one dimensional n^+-n-n^+ diode. Velocity u (upper), temperature T (middle left), concentration n (middle right), total energy W (lower left) and electric field $-\Phi'$ (lower right). Solid line: $r=-1$; dashed line: $r=-2$; circles: $r=-2$ in the coefficient of (2.7); pluses: $r=-2$ in (2.7)

The standard HD model uses $r = -1$ in the Wiedemann-Franz law (2.7) and the relaxation times (2.11). The numerical solution of this is shown as solid lines in Figure 8. We can clearly observe the spurious velocity overshoot at the right junction, but otherwise the solution is basically correct comparing with direct Monto-Carlo simulations (not shown). When r is taken as -2 in (2.7) and (2.11), the solution is completely wrong (dashed line in Figures 8). However, when one takes $r = -2$ only in the coefficient of κ in (2.7) but leaves $r = -1$ in the power of κ in (2.7) and in (2.11), i.e., when one uses

$$\kappa = \frac{1}{2} n \frac{k^2 \mu_0}{e} T \left(\frac{T}{T_0} \right)^{-1}, \quad (68)$$

in the place of (2.7) and leaves $r = -1$ in (2.11) unchanged, as was done in [10], one obtains a greatly reduced spurious overshoot (the circles in Figures 8). Finally, the result with $r = -2$ in κ in (2.7) but with $r = -1$ in (2.11) unchanged, is shown by pluses in Figure 8. We can see that the spurious overshoot also disappears.

7.3 RT model for a one dimensional diode

We present numerical simulation results for the RT model, described in Section 3, for the same one dimensional diode used in Subsection 7.2. Although the RT model is a parabolic system with two equations, the existence of sharp transition regions near the junctions justifies the usage of ENO shock capturing algorithms for the hyperbolic part.

In Figure 9, we show the results of velocity u , temperature T , concentration n , total energy E , and electric field $-\Phi'$ of the RT simulation, in circles, in a background of standard HD results ($r = -1$) in solid lines, and of HD results with $r = -2$ in the coefficient of κ in (2.7) but with $r = -1$ in the power (i.e., (2.7) is replaced by (7.1)), and $r = -1$ in (2.11), in dashed lines. We can see that the RT model greatly reduces the spurious velocity overshoot and is comparable with the result of the empirically modified HD result in dashed lines.

Extensive numerical tests about the RT model, as well as comparisons between the RT and HD models, constitute ongoing research, jointly with U. Ravaioli, E. Kan and D. Chen at the University of Illinois.

Acknowledgements: We would like to thank Edwin Kan, Umberto Ravaioli and Stanley Osher for helpful discussions. Computations were performed on the Cray YMP at the Pittsburgh Supercomputing Center and on the Cray YMP at the University of Illinois.

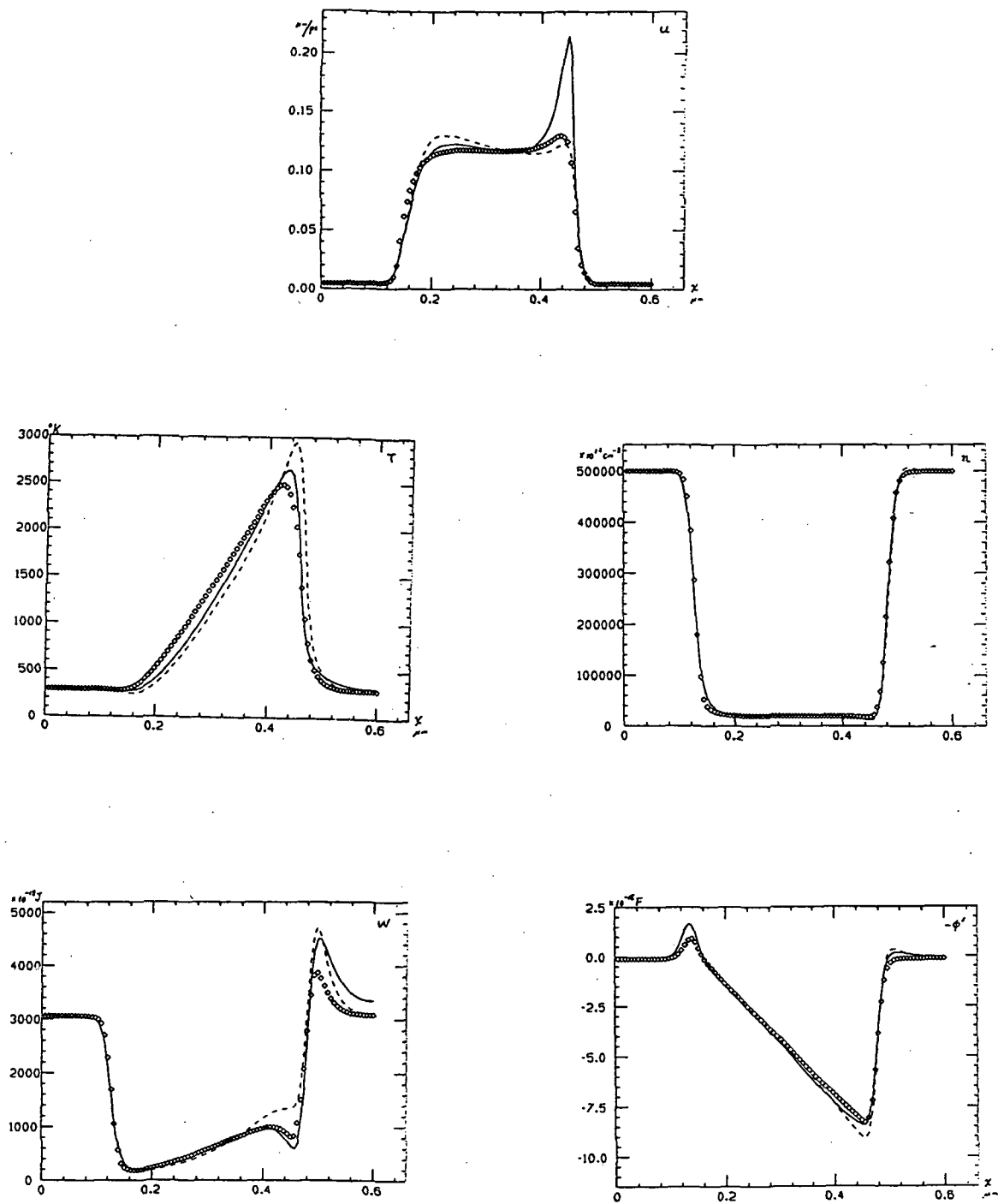


Figure 9: One dimensional n^+-n-n^+ diode. Velocity u (upper), temperature T (middle left), concentration n (middle right), total energy E (lower left), and electric field $-\Phi'$ (lower right). Solid line: standard HD with $r=-1$; circles: RT; dashed lines: HD with $r=-2$ in the coefficient of (2.7)

References

- [1] G. Baccarani and M. R. Wordeman. An investigation of steady-state velocity overshoot effects in Si and GaAs devices. *Solid State Electr.*, 28:407–416, 1985.
- [2] F. J. Blatt. *Physics of Electric Conduction in Solids*. McGraw Hill, New York, 1968.
- [3] K. Blotekjaer. Transport equations for electrons in two-valley semiconductors. *IEEE Trans. Electron Devices*, 17:38–47, 1970.
- [4] C. Cercignani. *The Boltzmann Equation and its Application*. Springer-Verlag, New York, 1987.
- [5] D. Chen, E. Kan, K. Hess, and U. Ravaioli. Steady-state macroscopic transport equations and coefficients for submicron device modeling. *To appear*.
- [6] E. Fatemi, C. Gardner, J. Jerome, S. Osher, and D. Rose. Simulation of a steady-state electron shock wave in a submicron semiconductor device using high order upwind methods. In K. Hess, J. P. Leburton, and U. Ravaioli, editors, *Computational Electronics*, pages 27–32. Kluwer Academic Publishers, 1991.
- [7] E. Fatemi, J. Jerome, and S. Osher. Solution of the hydrodynamic device model using high-order nonoscillatory shock capturing algorithms. *IEEE Transactions on Computer-Aided Design of Integrated Circuits and Systems*, CAD-10:232–244, 1991.
- [8] Irene M. Gamba. Stationary transonic solutions for a one-dimensional hydrodynamic model for semiconductors. *Communications in P.D.E.*
- [9] C. L. Gardner, J. W. Jerome, and D. J. Rose. Numerical methods for the hydrodynamic device model: Subsonic flow. *IEEE Transactions on Computer-Aided Design of Integrated Circuits and Systems*, CAD-8:501–507, 1989.
- [10] A. Gnudi, F. Odeh, and M. Rudan. An efficient discretization scheme for the energy continuity equation in semiconductors. In *Proceedings of SISDP*, pages 387–390, 1988.
- [11] W. Hänsch and M. Miura-Mattausch. The hot-electron problem in small semiconductor devices. *J. Appl. Phys.*, 60:650–656, 1986.
- [12] A. Harten, B. Engquist, S. Osher and S. Chakravarthy. Uniformly high order accurate essentially non-oscillatory schemes, III. *J. Comp. Phys.*, 71:231–303, 1987.

- [13] Joseph W. Jerome. Consistency of semiconductor modelling: An existence/stability analysis for the stationary van Roosbroeck system. *SIAM J. Appl. Math.*, 45(4):565–590, August 1985.
- [14] Joseph W. Jerome. Algorithmic aspects of the hydrodynamic and drift-diffusion models. In R. E. Bank, R. Bulirsch, and K. Merten, editor, *Mathematical Modelling and Simulation of Electrical Circuits and Semiconductor Devices*, pages 217–236. Birkhäuser Verlag, 1990.
- [15] Joseph W. Jerome and Thomas Kerkhoven. A finite element approximation theory for the drift-diffusion semiconductor model. *SIAM J. Num. Anal.*, 28:403–422, 1991.
- [16] Joseph W. Jerome and Thomas Kerkhoven. *Steady State Drift Diffusion Semiconductor Models*. SIAM, 1992.
- [17] M. S. Mock. On equations describing steady-state carrier distributions in a semiconductor device. *Comm. Pure Appl. Math.*, 25:781–792, 1972.
- [18] J. P. Nougier, J. Vaissiere, D. Gasquet, J. Zimmermann, and E. Constant. Determination of the transient regime in semiconductor devices using relaxation time approximations. *J. Appl. Phys.*, 52:825–832, 1981.
- [19] P. Roe. Approximate Riemann solvers, parameter vectors, and difference schemes. *J. Comp. Phys.*, 27:1–31, 1978.
- [20] M. Rudan and F. Odeh. Multi-dimensional discretization scheme for the hydrodynamic model of semiconductor devices. *COMPEL*, 5:149–183, 1986.
- [21] T. Seidman. Steady state solutions of diffusion reaction systems with electrostatic convection. *Nonlinear Anal.*, 4:623–637, 1980.
- [22] S. Selberherr. *Analysis and Simulation of Semiconductor Devices*. Springer-Verlag, Wien - New York, 1984.
- [23] C.-W. Shu, G. Erlebacher, T. Zang, D. Whitaker, and S. Osher. High-order ENO schemes applied to two- and three-dimensional compressible flow. ICASE Report 91-38, 1991. To appear in *J. Appl. Numer. Math.*
- [24] C.-W. Shu and S. J. Osher. Efficient implementation of essentially non-oscillatory shock capturing schemes. *J. Comp. Phys.*, 77:439–471, 1988.

- [25] C.-W. Shu and S. J. Osher. Efficient implementation of essentially non-oscillatory shock capturing schemes, II. *J. Comp. Phys.*, 83:32-78, 1989.

REPORT DOCUMENTATION PAGE

Form Approved
OMB No. 0704-0188

Public reporting burden for this collection of information is estimated to average 1 hour per response, including the time for reviewing instructions, searching existing data sources, gathering and maintaining the data needed, and completing and reviewing the collection of information. Send comments regarding this burden estimate or any other aspect of this collection of information, including suggestions for reducing this burden, to Washington Headquarters Services, Directorate for Information Operations and Reports, 1215 Jefferson Davis Highway, Suite 1204, Arlington, VA 22202-4302, and to the Office of Management and Budget, Paperwork Reduction Project (0704-0188), Washington, DC 20503.

1. AGENCY USE ONLY (Leave blank)	2. REPORT DATE October 1991	3. REPORT TYPE AND DATES COVERED Contractor Report	
4. TITLE AND SUBTITLE ENERGY MODELS FOR ONE-CARRIER TRANSPORT IN SEMICONDUCTOR DEVICES		5. FUNDING NUMBERS NAS1-18605 505-90-52-01	
6. AUTHOR(S) Joseph W. Jerome Chi-Wang Shu		8. PERFORMING ORGANIZATION REPORT NUMBER ICASE Report No. 91-78	
7. PERFORMING ORGANIZATION NAME(S) AND ADDRESS(ES) Institute for Computer Applications in Science and Engineering Mail Stop 132C, NASA Langley Research Center Hampton, VA 23665-5225		10. SPONSORING/MONITORING AGENCY REPORT NUMBER NASA CR-189549 ICASE Report No. 91-78	
9. SPONSORING/MONITORING AGENCY NAME(S) AND ADDRESS(ES) National Aeronautics and Space Administration Langley Research Center Hampton, VA 23665-5225		11. SUPPLEMENTARY NOTES Langley Technical Monitor: Michael F. Card Final Report To appear in IMA Volume in Mathematics and its Applications	
12a. DISTRIBUTION/AVAILABILITY STATEMENT Unclassified - Unlimited Subject Category 64		12b. DISTRIBUTION CODE	
13. ABSTRACT (Maximum 200 words) Simulations of the hydrodynamic model for semi-conductor device in one and two space dimensions, and simulations of a newly developed energy model, the RT model, are presented using essentially non-oscillatory (ENO) shock capturing algorithms. Comparisons between models are performed. Some mathematical results regarding those models are also presented.			
14. SUBJECT TERMS energy models; shock capturing algorithms; conservation laws; velocity overshoot; parabolic and nonparabolic energy bands		15. NUMBER OF PAGES 28	16. PRICE CODE A03
17. SECURITY CLASSIFICATION OF REPORT Unclassified	18. SECURITY CLASSIFICATION OF THIS PAGE Unclassified	19. SECURITY CLASSIFICATION OF ABSTRACT	20. LIMITATION OF ABSTRACT